DOI 10.1007/s10778-021-01070-w
*International Applied Mechanics, Vol. 57, No. 2, March, 2021*

# STRESS ANALYSIS OF HOLLOW ORTHOTROPIC CYLINDERS WITH OVAL CROSS-SECTION*

**Ya. M. Grigorenko[1] and L. S. Rozhok[2]**

**The stress state of hollow cylinders with oval cross-section made of orthotropic and isotropic materials is analyzed using spatial problem statement and analytical methods of separation of variables, approximation of functions by discrete Fourier series, and numerical discrete-orthogonalization method. The reference surface in the cross-section is described by the Cassini oval equation. The analytical results are presented in the form of plots and tables of distributions of displacements and stresses and analyzed.**

**Keywords:** Cassini ovals, discrete Fourier series, discrete-orthogonalization method, hollow orthotropic cylinder, oval cross-section, stress state

**Introduction.** Plates and shells of different thickness and shape are functional elements of structures in the aerospace industry, mechanical engineering, medicine, construction, etc. Under severe operating conditions, they are subject to static and dynamic loads, humidity, temperature, electric and magnetic fields [6, 8, 16–18, 21, 22]. To increase the resistance to external actions, such structures are made of composite materials [13, 23].

Recently, hollow panels with elliptic and oval cross-section have been widely used in construction and architecture [4, 7, 15, 25]. Such panels have aesthetic appearance and, due to different stiffness along the principal axes, they can be aligned so as to ensure the most effective resistance to loads [24].

The present paper continues studies that approximate functions by Fourier series in solving problems of the stress state of hollow orthotropic cylinders with noncircular cross-section [9–11].

**1. Problem Statement.** Let us consider a hollow cylinder using a curvilinear orthogonal coordinate system $(s, t, \gamma)$ with a reference surface in the plane $(s, t)$ and the coordinate $\gamma$ running along the normal to this surface [2].

The coordinate surface is the mid-surface equidistant from the lateral surfaces. The mid-surface in the cross-section is described by the Cassini oval equation [5, 19]:

$$\rho = c\sqrt{\cos 2\psi + \sqrt{\cos^2 2\psi + \left(\frac{a^4}{c^4} - 1\right)}}, \quad 0 \le \frac{c}{a} < 1, \quad a \ne 0, \tag{1.1}$$

[1]S. P. Timoshenko Institute of Mechanics, National Academy of Sciences of Ukraine, 3 Nesterova Str., Kyiv, 03057, Ukraine; e-mail: ayagrigorenko1991@gmail.com. [2]National Transport University, 1 Omelyanovicha-Pavlenka St., Kyiv, 01010, Ukraine; e-mail: r.l.s@ua.fm. Translated from Prikladnaya Mekhanika, Vol. 57, No. 2, pp. 45–57, March–April 2021. Original article submitted September 16, 2019.

* This study was sponsored by the budget program "Support for Priority Areas of Scientific Research" (KPKVK 6541230).

 

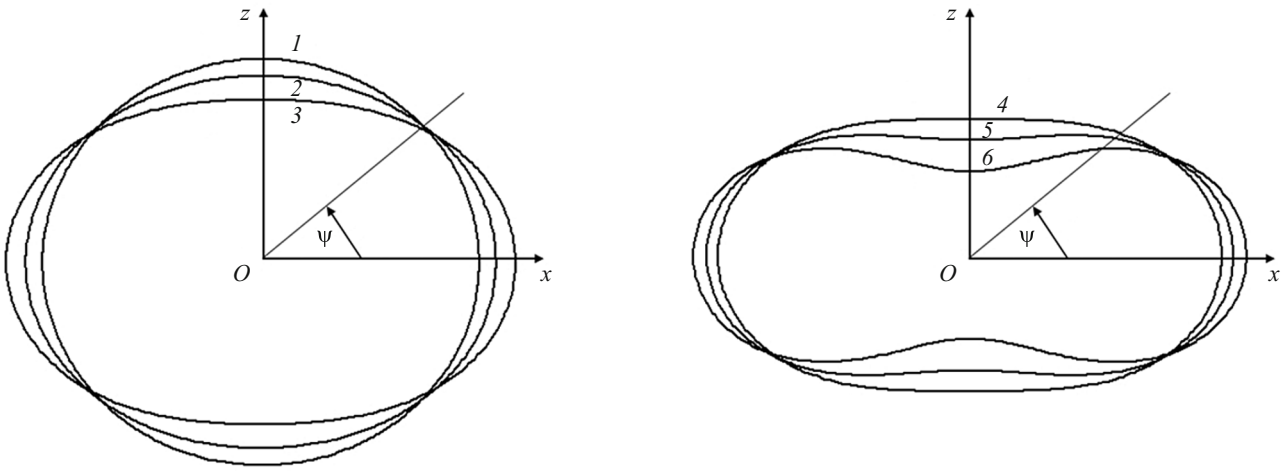


*a* *b*

Fig. 1

where ρ is the polar radius, ψ is an angle in the cross-section ($0 \le \psi \le 2\pi$), $c$ is the half-distance between the foci; $a$ is the product of distances between the foci and an arbitrary point. Varying the ratio $c/a$, we can change the cross-sectional shape into circular ($c = 0$, curve *1* in Fig. 1*a*), elliptic ($0 < c/a < 1/\sqrt{2}$, curves *2* and *3* in Fig. 1*a*), or oval ($1/\sqrt{2} \le c/a < 1$ curves *4–6* in Fig. 1*b*).

In the coordinate system chosen, the squared length of a linear element of the cylinder is given by

$$dS^2 = H_1^2 ds^2 + H_2^2 dt^2 + H_3^2 d\gamma^2,$$

where $H_1 = H_3 = 1$, $H_2 = 1 + [\gamma / R(t)]$ are Lode's parameters, $R(t) = R_t$ is the radius of curvature of the mid-surface directrix.

At its ends, the cylinder has diaphragms that are perfectly rigid in their plane and flexible beyond it. The boundary conditions at the ends are

$$\sigma_s = 0, \quad u_t = 0, \quad u_\gamma = 0 \quad \text{at} \quad s = 0, \ s = l. \tag{1.2}$$

The cylinder is subject to internal pressure uniformly distributed along the $t$ coordinate and varies along the generatrix as

$$q_\gamma = q_0 \sin(\pi s / l) \quad (q_0 = \text{const}).$$

The boundary conditions on the lateral surfaces are

$$\begin{aligned} &\sigma_\gamma = q_\gamma, \quad \tau_{s\gamma} = 0, \quad \tau_{t\gamma} = 0 \quad \text{at} \quad \gamma = \gamma_1, \\ &\sigma_\gamma = 0, \quad \tau_{s\gamma} = 0, \quad \tau_{t\gamma} = 0 \quad \text{at} \quad \gamma = \gamma_2. \end{aligned} \tag{1.3}$$

For cylinders of this class, all the stress factors satisfy periodicity conditions along the directrix:

$$\sigma_\gamma^i(s,t,\gamma) = \sigma_\gamma^i(s,t+T,\gamma); \quad \tau_{s\gamma}^i(s,t,\gamma) = \tau_{s\gamma}^i(s,t+T,\gamma);$$

$$\ldots \quad \ldots \quad \ldots \quad \ldots \quad \ldots; \quad u_t^i(s,t,\gamma) = u_t^i(s,t+T,\gamma),$$

where $T$ is the period.

We start with the equations of three-dimensional linear elasticity for an orthotropic body [20]. In setting up the governing system of differential equations, we assume that the directrix of the mid-surface is an arbitrary continuous curve without singularities and breaks, the mechanical characteristics can vary across the thickness remaining constant along the generatrix, and the distribution of the applied loads is arbitrary.

The functions in terms of which the boundary conditions on the lateral surfaces (1.3) are formulated are represented by the three stress components $\sigma_\gamma, \tau_{s\gamma}, \tau_{t\gamma}$ and three displacement components $u_\gamma, u_s, u_t$.

The governing system of partial differential equations with variable coefficients of the sixth order representing the spatial boundary-value problem in the domain $0 \le s \le l, t_1 \le t \le t_2, \gamma_1 \le \gamma \le \gamma_2$ follows from the above basic equations and takes the form

$$\frac{\partial \sigma_\gamma}{\partial \gamma} = (c_2 - 1)\frac{1}{H_2}\frac{\partial H_2}{\partial \gamma}\sigma_\gamma - \frac{\partial \tau_{s\gamma}}{\partial s} - \frac{1}{H_2}\frac{\partial \tau_{t\gamma}}{\partial t} + b_{22}\left(\frac{1}{H_2}\frac{\partial H_2}{\partial \gamma}\right)^2 u_\gamma$$

$$+ b_{12}\frac{1}{H_2}\frac{\partial H_2}{\partial \gamma}\frac{\partial u_s}{\partial s} + b_{22}\frac{1}{H_2^2}\frac{\partial H_2}{\partial \gamma}\frac{\partial u_t}{\partial t},$$

$$\frac{\partial \tau_{s\gamma}}{\partial \gamma} = -c_1\frac{\partial \sigma_\gamma}{\partial s} - \frac{1}{H_2}\frac{\partial H_2}{\partial \gamma}\tau_{s\gamma} - b_{12}\frac{1}{H_2}\frac{\partial H_2}{\partial \gamma}\frac{\partial u_\gamma}{\partial s} - b_{11}\frac{\partial^2 u_s}{\partial s^2}$$

$$- b_{66}\frac{1}{H_2}\frac{\partial}{\partial t}\left(\frac{1}{H_2}\frac{\partial u_s}{\partial t}\right) - (b_{12} + b_{66})\frac{1}{H_2}\frac{\partial^2 u_t}{\partial s \partial t},$$

$$\frac{\partial \tau_{t\gamma}}{\partial \gamma} = -c_2\frac{1}{H_2}\frac{\partial \sigma_\gamma}{\partial t} - \frac{2}{H_2}\frac{\partial H_2}{\partial \gamma}\tau_{t\gamma} - b_{22}\frac{1}{H_2}\frac{\partial}{\partial t}\left(\frac{1}{H_2}\frac{\partial H_2}{\partial \gamma}u_\gamma\right)$$

$$- (b_{12} + b_{66})\frac{1}{H_2}\frac{\partial^2 u_s}{\partial s \partial t} - b_{22}\frac{1}{H_2}\frac{\partial}{\partial t}\left(\frac{1}{H_2}\frac{\partial u_t}{\partial t}\right) - b_{66}\frac{\partial^2 u_t}{\partial s^2},$$

$$\frac{\partial u_\gamma}{\partial \gamma} = c_4\sigma_\gamma - c_2\frac{1}{H_2}\frac{\partial H_2}{\partial \gamma}u_\gamma - c_1\frac{\partial u_s}{\partial s} - c_2\frac{1}{H_2}\frac{\partial u_t}{\partial t},$$

$$\frac{\partial u_s}{\partial \gamma} = a_{55}\tau_{s\gamma} - \frac{\partial u_\gamma}{\partial s}, \quad \frac{\partial u_t}{\partial \gamma} = a_{44}\tau_{t\gamma} - \frac{1}{H_2}\frac{\partial u_\gamma}{\partial t} + \frac{1}{H_2}\frac{\partial H_2}{\partial \gamma}u_t \tag{1.4}$$

with the boundary conditions (1.2) and (1.3). The coefficients appearing in (1.4) are determined in terms of the mechanical characteristics of the cylinder material as follows:

$$b_{11} = a_{22}a_{66}/\Omega, \quad b_{12} = -a_{12}a_{66}/\Omega, \quad b_{22} = a_{11}a_{66}/\Omega,$$

$$b_{66} = (a_{11}a_{22} - a_{12}^2)/\Omega, \quad \Omega = (a_{11}a_{22} - a_{12}^2)a_{66},$$

$$c_1 = -(b_{11}a_{13} + b_{12}a_{23}), \quad c_2 = -(b_{12}a_{13} + b_{22}a_{23}), \quad c_4 = a_{33} + c_1a_{13} + c_2a_{23},$$

$$a_{11} = \frac{1}{E_s}, \quad a_{12} = -\frac{\nu_{st}}{E_t} = -\frac{\nu_{ts}}{E_s}, \quad a_{13} = -\frac{\nu_{s\gamma}}{E_\gamma} = -\frac{\nu_{\gamma s}}{E_s},$$

$$a_{22} = \frac{1}{E_t}, \quad a_{23} = -\frac{\nu_{\gamma t}}{E_t} = -\frac{\nu_{t\gamma}}{E_\gamma}, \quad a_{33} = \frac{1}{E_\gamma},$$

$$a_{44} = \frac{1}{G_{t\gamma}}, \quad a_{55} = \frac{1}{G_{s\gamma}}, \quad a_{66} = \frac{1}{G_{st}},$$

where $E_s, E_t, E_\gamma$ are the elastic moduli along the coordinate axes; $G_{t\gamma}, G_{s\gamma}, G_{st}$ are the shear moduli; $\nu_{t\gamma}, \nu_{s\gamma}, \nu_{st}, \nu_{\gamma t}, \nu_{\gamma s}$, and $\nu_{ts}$ are Poisson's ratios.

**2. Problem-Solving Method.** The technique for solving the spatial boundary-value problem for the system of equations (1.4) with the boundary conditions (1.2) and (1.3) is based on the approximation of the functions by discrete Fourier series [3] and consists of five stages.

To reduce the problem dimension at the first stage, by virtue of the boundary conditions (1.2), we apply the variable separation method. To this end, the components of loading and the unknown functions are expanded into Fourier series in the $s$ coordinate:

$$X(s,t,\gamma)=\sum_{n=1}^{N}X_n(t,\gamma)\sin\lambda_n s,$$

$$Y(s,t,\gamma)=\sum_{n=0}^{N}Y_n(t,\gamma)\cos\lambda_n s, \tag{2.1}$$

where $X=\{\sigma_\gamma,\tau_{t\gamma},u_\gamma,u_t,q_\gamma\}$, $Y=\{\tau_{s\gamma},u_s\}$, $\lambda_n=\dfrac{\pi n}{l}$ $(0\le s\le l)$.

Substituting series (2.1) into the governing system of equations (1.4) the boundary conditions (1.3) and separating the variables, we reduced the spatial boundary-value problem to a two-dimensional one for the amplitudes in series (2.1). The obtained system of differential equations, as well as (1.4), contains terms that are products of the unknown functions and coefficients dependent on two coordinates (running along the directrix and thickness) and make it impossible to separate the directrix variables. To overcome these difficulties, at the second stage, these terms in the governing system of equations are replaced by complementary functions (hereafter the index $n$ in the notation of the unknown functions and loading components is omitted):

$$\varphi_1^j=\frac{1}{H_2R_t}\left\{\sigma_\gamma;\tau_{s\gamma};u_\gamma;u_s;\frac{1}{H_2R_t}u_\gamma\right\}\quad\left(j=\overline{1,5}\right),$$

$$\varphi_2^j=\frac{1}{H_2R_t}\{\tau_{t\gamma};u_t\}\quad\left(j=\overline{1,2}\right),\qquad\varphi_3^j=\frac{1}{H_2}\left\{\frac{\partial\sigma_\gamma}{\partial t};\frac{\partial u_\gamma}{\partial t};\frac{\partial u_s}{\partial t}\right\}\quad\left(j=\overline{1,3}\right),$$

$$\varphi_4^j=\frac{1}{H_2}\left\{\frac{\partial\tau_{t\gamma}}{\partial t};\frac{\partial u_t}{\partial t};\frac{1}{R_t}\frac{\partial u_t}{\partial t}\right\}\quad\left(j=\overline{1,3}\right),$$

$$\varphi_5=\frac{1}{H_2}\frac{\partial}{\partial t}\varphi_1^3,\qquad\varphi_6=\frac{1}{H_2}\frac{\partial}{\partial t}\varphi_3^3,\qquad\varphi_7=\frac{1}{H_2}\frac{\partial}{\partial t}\varphi_4^2. \tag{2.2}$$

The governing system of equations with the complementary functions (2.2) takes the form

$$\frac{\partial\sigma_\gamma}{\partial\gamma}=(c_2-1)\varphi_1^1+\lambda_n\tau_{t\gamma}-\varphi_4^1+b_{22}\varphi_1^5+b_{12}\lambda_n\varphi_1^4+b_{22}\varphi_4^3,$$

$$\frac{\partial\tau_{s\gamma}}{\partial\gamma}=-c_1\lambda_n\sigma_\gamma-\varphi_1^2-b_{12}\lambda_n\varphi_1^3+b_{11}\lambda_n^2u_s-b_{66}\varphi_6-(b_{12}+b_{66})\lambda_n\varphi_4^2,$$

$$\frac{\partial\tau_{t\gamma}}{\partial\gamma}=-c_2\varphi_3^1-2\varphi_2^1-b_{22}\varphi_5+(b_{12}+b_{66})\lambda_n\varphi_3^3-b_{22}\varphi_7-b_{66}\lambda_n^2u_t,$$

$$\frac{\partial u_\gamma}{\partial\gamma}=c_4\sigma_\gamma-c_2\varphi_4^2+c_1\lambda_nu_s-c_2\varphi_1^3,$$

$$\frac{\partial u_s}{\partial \gamma} = a_{55}\tau_{s\gamma} - \lambda_n u_\gamma, \qquad \frac{\partial u_t}{\partial \gamma} = a_{44}\tau_{t\gamma} - \varphi_3^2 + \varphi_2^2 \tag{2.3}$$

with the boundary conditions

$$\sigma_\gamma = q_\gamma, \quad \tau_{s\gamma} = 0, \quad \tau_{t\gamma} = 0 \quad \text{at} \quad \gamma = \gamma_1,$$
$$\sigma_\gamma = 0, \quad \tau_{s\gamma} = 0, \quad \tau_{t\gamma} = 0 \quad \text{at} \quad \gamma = \gamma_2. \tag{2.4}$$

Formally, the coefficients of the system of equations (2.3) are independent of the coordinate $t$ and make it possible to separate the associated variables. To this end, at the third stage, the unknown and complementary functions and the loading components are expanded into Fourier series in the $t$ coordinate:

$$\widetilde{X}(t,\gamma) = \sum_{k=0}^{K} \widetilde{X}_k(\gamma)\cos\lambda_k t, \quad \widetilde{Y}(t,\gamma) = \sum_{k=1}^{K} \widetilde{Y}_k(\gamma)\sin\lambda_k t,$$

$$\lambda_k = \frac{2k\pi}{T} \quad (t_1 \le t \le t_2),$$

$$\widetilde{X} = \left\{\sigma_\gamma, \tau_{s\gamma}, u_\gamma, u_s, \varphi_1^j, \varphi_4^j, \varphi_6, q_\gamma\right\}, \quad \widetilde{Y} = \left\{\tau_{t\gamma}, u_t, \varphi_2^j, \varphi_3^j, \varphi_5, \varphi_7\right\}. \tag{2.5}$$

Substituting series (2.5) into the governing system of equations (2.3) and the boundary conditions (2.4) and separating the variables, we arrive at a one-dimensional boundary-value problem for the amplitudes of series (2.5), which is described by the system of ordinary differential equations with constant coefficients

$$\frac{d\sigma_{\gamma,k}}{d\gamma} = \lambda_n \tau_{s\gamma,k} + (c_2 - 1)\varphi_{1,k}^1 - \varphi_{4,k}^1 + b_{22}\varphi_{1,k}^5 + b_{12}\lambda_n \varphi_{1,k}^4 + b_{22}\varphi_{4,k}^3,$$

$$\frac{d\tau_{s\gamma,k}}{d\gamma} = -c_1\lambda_n\sigma_{\gamma,k} + b_{11}\lambda_n^2 u_{s,k} - \varphi_{1,k}^2 - b_{12}\lambda_n\varphi_{1,k}^3 - b_{66}\varphi_{6,k} - (b_{12} + b_{66})\lambda_n\varphi_{4,k}^2,$$

$$\frac{d\tau_{t\gamma,k}}{d\gamma} = b_{66}\lambda_n^2 u_{t,k} - c_2\varphi_{3,k}^1 - 2\varphi_{2,k}^1 - b_{22}\varphi_{5,k} - (b_{12} + b_{66})\lambda_n\varphi_{3,k}^3 - b_{22}\varphi_{7,k},$$

$$\frac{du_{\gamma,k}}{d\gamma} = c_4\sigma_{\gamma,k} + c_1\lambda_n u_{s,k} - c_2\varphi_{4,k}^2 - c_2\varphi_{1,k}^3,$$

$$\frac{du_{s,k}}{d\gamma} = a_{55}\tau_{s\gamma,k} - \lambda_n u_{\gamma,k}, \qquad \frac{du_{t,k}}{d\gamma} = a_{44}\tau_{t\gamma,k} - \varphi_{3,k}^2 + \varphi_{2,k}^2 \quad \left(k = \overline{0,K}\right) \tag{2.6}$$

with the boundary conditions

$$\sigma_{\gamma,k} = q_{\gamma,k}, \quad \tau_{s\gamma,k} = 0, \quad \tau_{t\gamma,k} = 0 \quad \text{at} \quad \gamma = \gamma_1,$$
$$\sigma_{\gamma,k} = 0, \quad \tau_{s\gamma,k} = 0, \quad \tau_{t\gamma,k} = 0 \quad \text{at} \quad \gamma = \gamma_2. \tag{2.7}$$

To integrate this system of equations, at the fourth stage, we employ the stable numerical method of discrete orthogonalization [1] for all harmonics of series (2.5) simultaneously. Since the number of unknowns in the governing system (2.6) exceeds the number of equations (due to the complementary functions), the system of equations at each step of the numerical method is closed by calculating the amplitudes of the complementary functions from the current values of the amplitudes of the unknown functions at the fifth stage by approximating them by discrete Fourier series [14]. To this end, we set up tables of values of the complementary functions at a number of points $t_i$ $(i = \overline{1,R})$ of the directrix for a fixed value of the thickness coordinate using the following formulas:

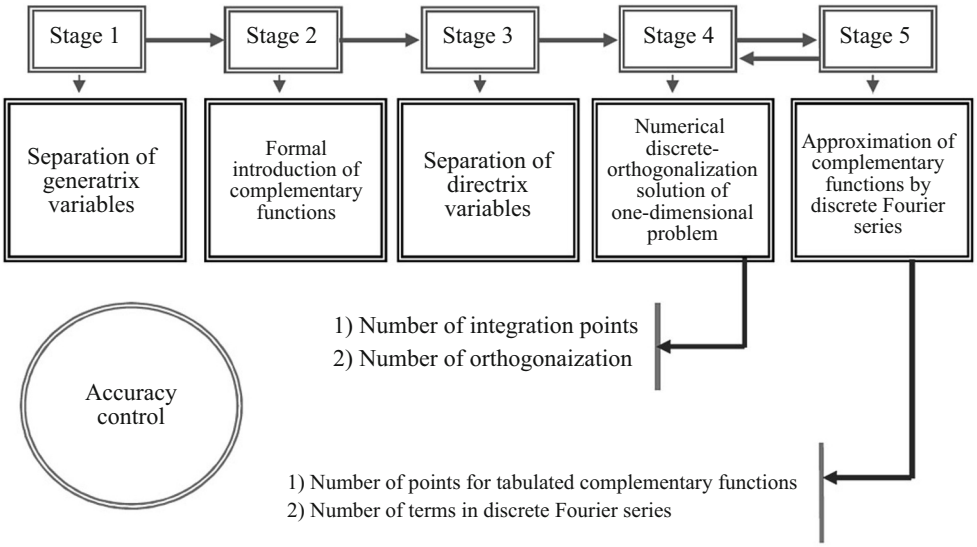


Fig. 2

$$h_1^i = \frac{1}{H_2}\frac{\partial H_2}{\partial \gamma} = \frac{1}{R_t(t_i)+\gamma_k}, \quad h_2^i = \frac{1}{H_2} = \frac{R_t(t_i)}{R_t(t_i)+\gamma_k},$$

$$\varphi_{1,i}^j = h_1^i \sum_{m=0}^{M} \left\{ \sigma_{\gamma,m};\ \tau_{s\gamma,m};\ u_{\gamma,m};\ u_{s,m} \right\} \cos \lambda_m t_i \qquad (j = \overline{1,4}),$$

$$\varphi_{1,i}^5 = \left(h_1^i\right)^2 \sum_{m=0}^{M} u_{\gamma,m} \cos \lambda_m t_i,$$

$$\varphi_{2,i}^j = h_1^i \sum_{m=0}^{M} \left\{ \tau_{t\gamma,m};\ u_{t,m} \right\} \sin \lambda_m t_i \qquad (j = 1,2),$$

$$\varphi_{3,i}^j = -h_2^i \sum_{m=0}^{M} \lambda_m \left\{ \sigma_{\gamma,m};\ u_{\gamma,m};\ u_{s,m} \right\} \sin \lambda_m t_i \quad (j = \overline{1,3}),$$

$$\varphi_{4,i}^j = h_2^i \sum_{m=0}^{M} \lambda_m \left\{ \tau_{t\gamma,m};\ u_{t,m} \right\} \cos \lambda_m t_i \qquad (j = 1,2),$$

$$\varphi_{4,i}^3 = h_1^i h_2^i \sum_{m=0}^{M} \lambda_m u_{t,m} \cos \lambda_m t_i, \qquad \varphi_{5,i} = -h_2^i \sum_{m=0}^{M} \lambda_m \varphi_{1,m}^3 \sin \lambda_m t_i,$$

$$\varphi_{6,i} = h_2^i \sum_{m=0}^{M} \lambda_m \varphi_{3,m}^3 \cos \lambda_m t_i, \qquad \varphi_{7,i} = -h_2^i \sum_{m=0}^{M} \lambda_m \varphi_{4,m}^2 \sin \lambda_m t_i.$$

Next, using the standard procedure of determining the Fourier coefficients of tabulated functions, we determine these coefficients. Substituting them into the governing system of equations (2.6), we go to the next step of integration. At the beginning of integration, the amplitudes of the complementary functions are determined from the amplitudes of the unknown functions in accordance with the boundary conditions (2.7).

TABLE 1

| $u_\gamma E_0 / q_0$ ($\gamma = 0$) | | | | | |
|---|---|---|---|---|---|
| $L^i$ | $L^o$ | $c = 12$ | | $c = 16$ | |
| | | $\psi = 0$ | $\psi = \pi / 2$ | $\psi = 0$ | $\psi = \pi / 2$ |
| 4 | 4 | –255.367 | 841.678 | –600.247 | 3066.88 |
| 8 | 4 | –254.360 | 842.721 | –599.232 | 3067.19 |
| | 8 | –254.359 | 842.720 | –599.219 | 3067.09 |
| 32 | 8 | –254.356 | 842.720 | –599.228 | 3067.15 |
| | 16 | –254.360 | 842.721 | –599.226 | 3067.12 |
| | 32 | –254.360 | 842.721 | –599.225 | 3067.12 |

TABLE 2

| $\sigma_\psi / q_0$ | | | | | |
|---|---|---|---|---|---|
| $L^i$ | $L^o$ | $c = 12$ ($\gamma = h/2$) | | $c = 16$ ($\gamma = -h/2$) | |
| | | $\psi = 0$ | $\psi = \pi/2$ | $\psi = 0$ | $\psi = \pi/2$ |
| 4 | 4 | –14.3303 | 26.5745 | –4.64614 | –92.2256 |
| 8 | 4 | –14.2300 | 27.5761 | –4.74678 | –92.3335 |
| | 8 | –14.2299 | 27.5670 | –4.74677 | –92.3325 |
| 32 | 8 | –14.2298 | 27.5761 | –4.74698 | –92.3342 |
| | 16 | –14.2299 | 27.5761 | –4.74679 | –92.3334 |
| | 32 | –14.2299 | 27.5761 | –4.74679 | –92.3334 |

**3. Estimation of Accuracy of the Results.** Since the cylinder mid-surface in the cross-section is described in the polar coordinates $(\rho, \psi)$, it is necessary to use an appropriate transformation coefficient when changing from the coordinate $t$ to the coordinate $\psi$. For example, for an arbitrary function $V(t(\psi), \gamma)$, we have

$$\frac{dt}{d\psi} = \sqrt{\rho^2 + \left(\frac{d\rho}{d\psi}\right)^2} = \omega(\psi), \qquad \frac{\partial V}{\partial \psi} = \frac{\partial V}{\partial t}\frac{dt}{d\psi}, \qquad \frac{\partial V}{\partial t} = \frac{1}{\omega(\psi)}\frac{\partial V}{\partial \psi}.$$

The radius of curvature of the mid-surface is given by

$$R(\psi) = \omega^3(\psi) \Big/ \left(\rho^2 + 2\rho'^2 + \rho\rho''\right).$$

The above problem-solving technique consists of five stages (Fig. 2). The error appears at the last two stages due to the use of the numerical method and discrete Fourier series. The accuracy of the results is controlled by varying the number of

TABLE 3

| $u_\gamma E_0 / q_0$ ($\gamma = 0$) | | | | | |
|---|---|---|---|---|---|
| $M$ | $R$ | $c = 12$ | | $c = 16$ | |
| | | $\psi = 0$ | $\psi = \pi/2$ | $\psi = 0$ | $\psi = \pi/2$ |
| 4 | 20 | –90.6204 | 446.946 | 6.85213 | 495.954 |
| | 60 | –90.6214 | 446.967 | 6.85237 | 495.951 |
| | 80 | –90.6225 | 446.987 | 6.85234 | 495.950 |
| 12 | 20 | –254.579 | 843.080 | –627.839 | 3103.92 |
| | 60 | –254.396 | 842.733 | –596.458 | 3066.04 |
| | 80 | –254.346 | 842.727 | –596.461 | 3067.06 |
| 17 | 60 | –254.361 | 842.723 | –599.227 | 3067.14 |
| | 80 | –254.360 | 842.721 | –599.226 | 3067.12 |
| | 100 | –254.360 | 842.721 | –599.226 | 3067.12 |

TABLE 4

| $\sigma_\psi / q_0$ | | | | | |
|---|---|---|---|---|---|
| $M$ | $R$ | $c = 12$ ($\gamma = h/2$) | | $c = 16$ ($\gamma = -h/2$) | |
| | | $\psi = 0$ | $\psi = \pi/2$ | $\psi = 0$ | $\psi = \pi/2$ |
| 4 | 20 | –6.46957 | 12.9310 | –1.37431 | –18.8625 |
| | 60 | –6.46950 | 12.9318 | –1.37410 | –18.8624 |
| | 80 | –6.46948 | 12.9326 | –1.37426 | –18.8620 |
| 12 | 20 | –14.2410 | 27.5935 | –5.46985 | –92.1152 |
| | 60 | –14.2304 | 27.5833 | –5.02654 | –93.4312 |
| | 80 | –14.2300 | 27.5756 | –5.02659 | –92.4316 |
| 17 | 60 | –14.2298 | 27.5760 | –4.74677 | –92.3332 |
| | 80 | –14.2299 | 27.5761 | –4.74679 | –92.3334 |
| | 100 | –14.2299 | 27.5761 | –4.74679 | –92.3334 |

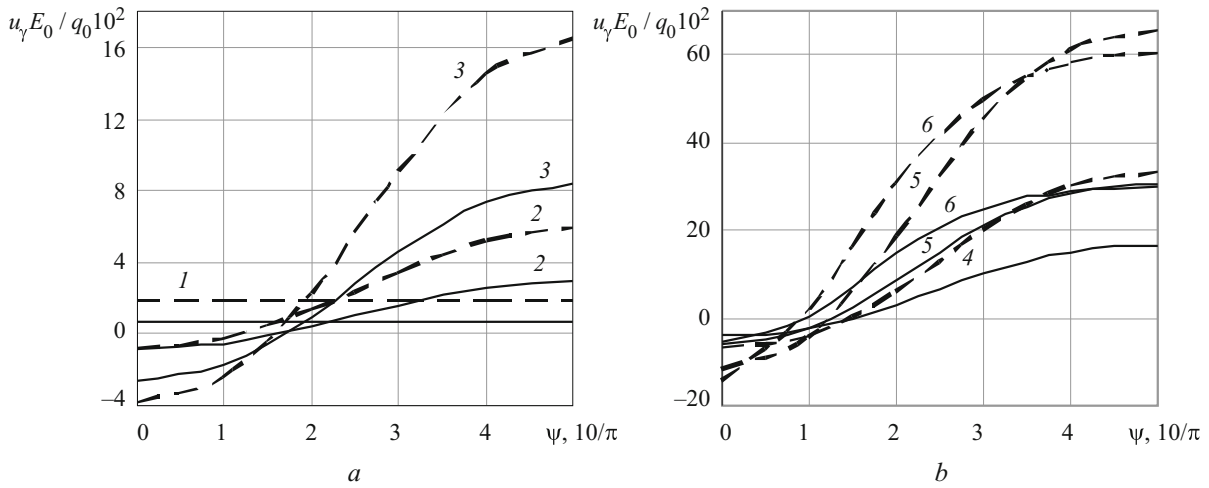


*a* *b*

Fig. 3

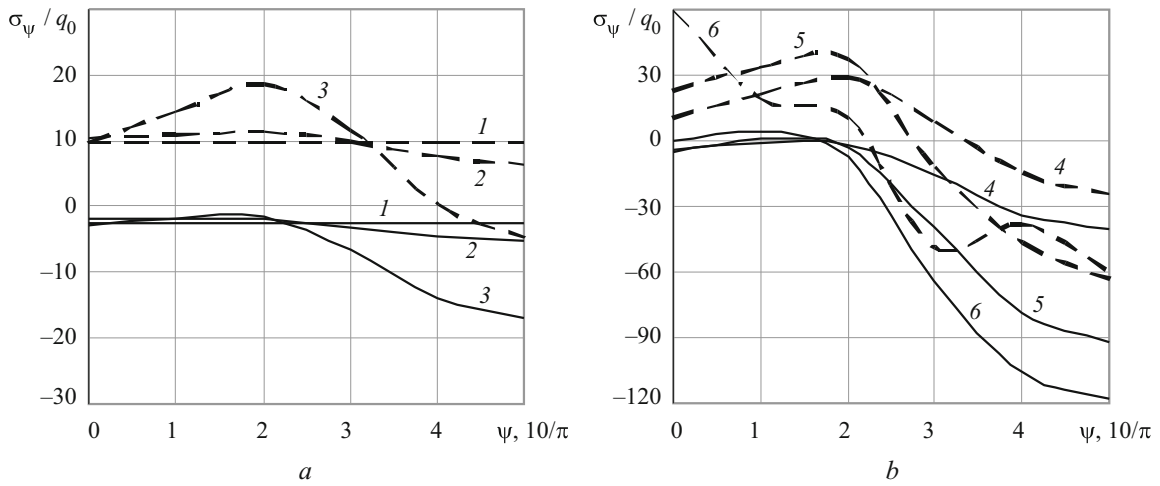


*a* *b*

Fig. 4

integration points and orthogonolization in the numerical method and by varying the number of points on the directrix used to tabulate the complementary functions and the number of terms in the discrete Fourier series.

To estimate the accuracy of the results, we will determine the stress state of a hollow cylinder with cross-section described by the Cassini oval equation (1.1). The cylinder is made of an orthotropic material and subject to internal pressure. Input data are: cylinder length $l = 40$; thickness $h = 2$; $a = 20$, $c = 12$ and 16 (curves *3* and *5* in Fig. 1, respectively):

$$E_s = 3.68E_0, \quad E_\psi = 2.68E_0, \quad E_\gamma = 1.1E_0, \quad \nu_{s\psi} = 0.105, \quad \nu_{s\gamma} = 0.405,$$

$$\nu_{\psi\gamma} = 0.431, \quad G_{s\psi} = 0.5E_0, \quad G_{s\gamma} = 0.45E_0, \quad G_{\psi\gamma} = 0.41E_0.$$

The results obtained in the middle (along the cylinder length) cross-section are summarized in Tables 1–4. The accuracy of the results obtained with the discrete-orthogonalization method is estimated in Tables 1 and 2, and the accuracy of the results obtained by approximating the complementary functions by discrete Fourier series is estimated in Tables 3 and 4.

Tables 1 and 3 present the values of the normal displacements $u_\gamma$, while Tables 2 and 4 summarize stresses $\sigma_\psi$ in sections across the thickness. The displacement values are given for the reference surface ($\gamma = 0$), while the stresses are given for cylinders with $c = 12$ on the outer surface ($\gamma = h/2$) and for cylinders with $c = 16$ on the inner surface ($\gamma = -h/2$), where their amplitudes are maximum.

As can be seen, the results are accurate up to the fifth or sixth decimal places with 32 integration points ($L^i$) and 16 orthogonalization points ($L^o$).

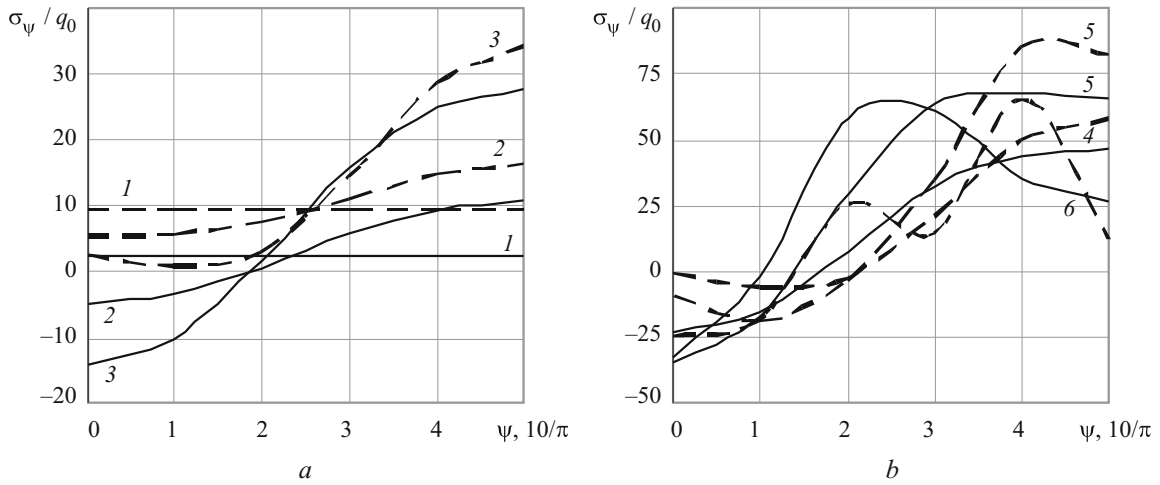


Fig. 5

From Tables 3 and 4 it follows that the results are accurate up to the fourth or fifth decimal places with 80 points ($R$) on the directrix for tabulated values of the complementary functions and 17 terms ($M$) of the discrete Fourier series.

**4. Analysis of the Numerical Results.** Using the above approach, we have solved the problem of the stress state of hollow orthotropic cylinders whose cross-sectional mid-surface described by the Cassini oval equation (1.1). The cylinders are subject to internal pressure.

The input data: cylinder length $l = 40$; thickness $h = 2$; $a = 20$, $c = 0$, 8, 12, 14, 16, 18; the mechanical characteristics of the material: $E_s = 3.68E_0$, $E_\psi = 2.68E_0$, $E_\gamma = 1.1E_0$, $G_{s\psi} = 0.5E_0$, $G_{\psi\gamma} = 0.41E_0$, $G_{s\gamma} = 0.45E_0$, $\nu_{s\psi} = 0105$, $\nu_{\psi\gamma} = 0.431$, $\nu_{s\gamma} = 0.405$.

Let us compare the stress state characteristics of these cylinders with those of isotropic cylinders with Young's modulus $E = E_0$ and Poisson's ratio $\nu = 0.3$.

The results obtained are shown in Fig. 3 for the normal displacements $u_\gamma$ of the reference surface ($\gamma = 0$), in Fig. 4 for the stresses $\sigma_\psi$ on the inner surface ($\gamma = -h/2$), and in Fig. 5 for the stresses on the outer surface ($\gamma = h/2$). Here the dashed curves refer to the isotropic cylinders, while the solid curves refer to the orthotropic ones. The curves representing different shapes of the cylinder cross-section (Fig. 1) are denoted by *1–6*.

From Fig. 3 we can see that the use of orthotropic maximal reduces the maximum normal displacements by a factor of 2 to 2.5 for all shapes of the cross-section.

The deviation of the cross-sectional shape from circular results in the redistribution of the displacements $u_\gamma$ along the directrix. In the section $\psi = \pi/2$, the amplitude of the normal displacements is greater than in the section $\psi = 0$ by a factor of 3.7 for shape 2, by a factor of 3.3 for shape 3, by a factor of 4.1 for shape 4, by a factor of 5 for shape 5, and by a factor of 5.4 for shape 6. The maximal displacement increases by a factor of 4 for shape 2, by a factor of 11.3 for shape 3, by a factor of 22.5 for shape 4, by a factor of 41.4 for shape 5, and by a factor of 40.4 for shape 6, compared with the circular cylinder (shape 1).

The distribution of stresses along the directrix is as follows (Figs. 4 and 5). The amplitude of the stress $\sigma_\psi$ for isotropic material is maximum on the unloaded outer surface, in the section $\psi = \pi/2$ for shapes 2–5, and in the section $\psi = 2\pi/5$ for shape 6. In the case of orthotropic material, the stress amplitude is maximum in the section $\psi = \pi/2$ for shapes 2–5 on the outer surface and for shapes 5 and 6 on the inner surface. The use of orthotropic material cylinders reduces the maximum amplitude by a factor of 1.2 to 1.5 for shapes 2–4 and increases the maximum amplitude by a factor of 1.2 to 1.8 for shapes 5 and 6.

The greater the deviation of the cross-section from circular, the stronger the nonlinearity of the distribution of stresses $\sigma_\psi$ for both materials.

Figure 6 demonstrates the distribution of the stress $\sigma_\psi$ across the thickness of the orthotropic cylinder with oval cross-section in various sections of the directrix for shape 2 (Fig. 6*a*), shape 3 (Fig. 6*b*), shape 4 (Fig. 6*c*), shape 5 (Fig. 6*d*), and shape 6 (Fig. 6*e*). Some sections of the directrix spaced at $\pi/10$ within the interval $0 \le \psi \le \pi/2$ are denoted by *1–6*.

From Fig. 6, we can see that the stresses $\sigma_\psi$ are distributed linearly over the thickness. The stresses on the inner surface for curves *1–3* hardly differ for all cross-sectional shapes. The same is true of straight lines *4–6* for shape 2 (Fig. 6*a*). For shape 5 (Fig. 6d), the stresses on the outer surface for straight lines *4–6* are very similar.

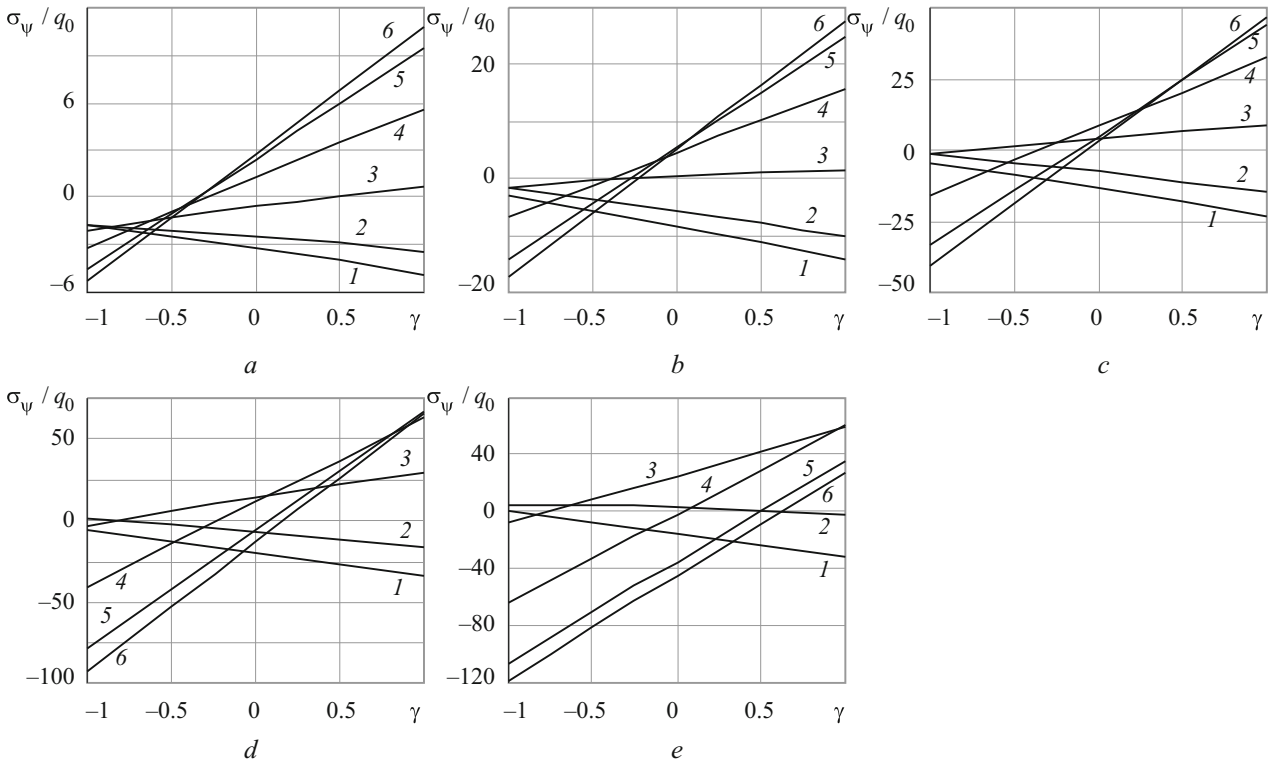


Fig. 6

The stress amplitudes on the outer and inner surfaces in the section $\psi = \pi / 2$ for shape 4 (Fig. 6*c*) are almost equal. The stresses are much greater on the outer surface for shapes 2 and 3 (Figs. 6*a* and 6*b*) and on the inner surface for shapes 5 and 6.

**Conclusions.** The spatial problem of the stress state of hollow orthotropic cylinders with mid-surface described by the Cassini oval equation has been solved by approximating the functions by discrete Fourier series. The accuracy of the results obtained with this method and the numerical method of discrete orthogonalization has been estimated. It has been shown that adequate accuracy can be achieved by increasing the number of integration and orthogonalization points and by varying the number of tabulated values of the complementary functions and the number of terms in the Fourier series.

The stress state of cylinders made of an isotropic material has been analyzed. It has been shown that varying the cross-sectional shape in combination with the use of an orthotropic material results in substantial redistribution of the stress state parameters. The results obtained can be used to select the optimal geometrical and mechanical parameters of functional elements of cylindrical shell structures with oval cross-section.

## REFERENCES


1. S. K. Godunov, "Numerical solution of boundary-value problems for systems of linear ordinary differential equations," *Usp. Mat. Nauk*, **16**, No. 3, 171–174 (1961).
2. Ya. M. Grigorenko, A. T Vasilenko, I. G. Emel'yanov, et. al., *Statics of Structural Members*, Vol. 8 of the twelve-volume series *Mechanics of Composites* [in Russian], A.S.K., Kyiv (1999).
3. Ya. M. Grigorenko, G. G. Vlaikov, and A. Ya. Grigorenko, *Numerical-Analytical Solution of Shell-Mechanics Problems Using Various Models* [in Russian], Academperiodika, Kyiv (2006).
4. L. P. Zheleznov, V. V. Kabanov, and D. V. Boiko, "Nonlinear deformation and stability of oval cylindrical shells under simple bending with internal pressure," *Prikl. Mekh. Tekhn. Fiz.*, **47**, No. 3, 119–125 (2006).
5. A. A. Savelov, *Plane Curves. Systematics*, *Properties*, *Application* [in Russian], Fizmatlit, Moscow (1960).
6. E. I. Bespalova and N. P. Boreiko, "Determination of the natural frequencies of compound shell systems using various deformation models," *Int. Appl. Mech.*, **55**, No. 1, 41–54 (2019).

7. L. Gardner, “Structural behavior of oval hollow sections,” *Advanced Steel Constr.*, **1**, No. 2, 29–54 (2005).
8. P. V. Gerasimenko and V. A. Khodakovskiy, “Numerical algorithm for investigating the stress–strain state of cylindrical shells of railway tanks,” *Vestnik St. Petersburg Univ.*, *Math.*, **52**, No. 2, 207–213 (2019).
9. Ya. M. Grigorenko and L. S. Rozhok, “Influence of orthotropy parameters on the stress state of hollow cylinders with elliptic cross-section,” *Int. Appl. Mech.*, **43**, No. 12, 1372–1379 (2007).
10. Ya. M. Grigorenko and L. S. Rozhok, “Stress analysis of circumferentially corrugated hollow orthotropic cylinders,” *Int. Appl. Mech.*, **42**, No. 12, 1389–1397 (2006).
11. Ya. M. Grigorenko and L. S. Rozhok, “Stress analysis of hollow elliptic cylinders with variable eccentricity and thickness,” *Int. Appl. Mech.*, **38**, No. 8, 954–966 (2002).
12. Ya. M. Grigorenko and L. S. Rozhok, “Stress–strain analysis of rectangular plates with a variable thickness and constant weight,” *Int. Appl. Mech.*, **38**, No. 2, 167–173 (2002).
13. A. N. Guz, “Nonclassical problems of fracture/failure mechanics: on the occasion of the 50th anniversary of the research (Review),” *Int. Appl. Mech.*, **55**, No. 2, 129–174 (2019).
14. R. W. Hamming, *Numerical Methods for Scientists and Engineers*, McGraw-Hill, New York (1962).
15. P. Jasion and K. Magnucki, “Elastic buckling of Cassini ovaloidal shells under external pressure—theoretical study,” *Archiv. Mech.*, **67**, No. 2, 179–192 (2015).
16. M. Karimiasl, “Chaotic dynamics of a non-autonomous nonlinear system for a smart composite shell subjected to the hygro-thermal environment,” *Microsyst. Technol.*, **25**, No. 7, 2587–2607 (2019).
17. K. G. Khoroshev, “Electroelastic state of an infinite multiply connected piezoelectric plate with known electric potentials applied to its boundaries,” *Int. Appl. Mech.*, **46**, No. 6, 687–695 (2010).
18. K. G. Khoroshev and Yu. A. Glushchenko, “The two-dimensional electroelasticity problems for multiconnected bodies situated under electric potential difference action,” *Int. J. Solids Struct.*, **49**, No. 18, 2703–2711 (2012).
19. G. A. Korn and T. M. Korn, *Mathematical Handbook for Scientists and Engineers*, McGraw-Hill, New York (1961).
20. S. G. Lekhnitsky, *Theory of an Anisotropy Body* [in Russian], Mir, Moscow (1981).
21. J. S. Mohamed Ali, S. Alsubari, and Y. Aminanda, “Hygrothermoelastic analysis of orthotropic cylindrical shells,” *Lat. Am. J. Solids Struct.*, **13**, No. 3, 573–589 (2016).
22. L. V. Mol’chenko and I. I. Loos, “Thermomagnetoelastic deformation of flexible isotropic shells of revolution subject to Joule heating,” *Int. Appl. Mech.*, **55**, No. 1, 68–78 (2019).
23. Y. Muramatsu and M. Shimoda, “Distributed-parametric optimization approach for free-orientation of laminated shell structures with anisotropic materials,” *Struct. Multidiscipl. Optimiz.*, **59**, No. 6, 1915–1934 (2019).
24. A. M. Ruiz-Teran and L. Gardner, “Elastic buckling of elliptical tubes,” *Thin-Walled Struct.*, **46**, 1304–1318 (2008).
25. N. Silvestre, “Buckling behavior of elliptical cylindrical shells and tubes under compression,” *Int. J. Solids Struct.*, **45**, 4427–4447 (2008).